Design Aspects of High-Speed Electrical Machines With Active Magnetic Bearings for Compressor Applications

Nikita Uzhegov, *Member, IEEE*, Alexander Smirnov, *Member, IEEE*, Cheol Hoon Park, Ji Hun Ahn, Janne Heikkinen, and Juha Pyrhönen, *Member, IEEE*

***Abstract*—Two-stage oil-free centrifugal air compressors can bring significant advantages and open new market opportunities for compressor manufacturers. One of the core technologies behind this compressor type is the high-speed electrical machine supported by active magnetic bearings. In this paper, the requirements set by the compressor on the electrical machine design are presented. The design solutions aimed to satisfy these requirements are discussed. Two case studies illustrate possible design approaches for the target application with examples of a 120-kW, 60 000-r/min induction machine with a solid rotor and a 225-kW, 50 000-r/min permanent-magnet synchronous machine (PMSM) with a full cylindrical magnet. The system design and simulation results are confirmed by measurements of a PMSM prototype.**

***Index Terms*—AC machine, active magnetic bearing (AMB), compressors, electrical design, high-speed (HS) drive, induction machines (IM), permanent magnet (PM) machines.**

Manuscript received December 9, 2016; revised February 18, 2017, March 16, 2017, and March 29, 2017; accepted April 5, 2017. Date of publication June 5, 2017; date of current version October 9, 2017. This work was supported in part by the Department of Chemical and Metallurgical Engineering of Aalto University and in part by the School of Energy Systems of Lappeenranta University of Technology. *(Corresponding author: Alexander Smirnov.)*

N. Uzhegov was with the Department of Electrical Engineering, School of Energy Systems, Lappeenranta University of Technology 53850, Lappeenranta, Finland. He is now with SpinDrive 54100, Lappeenranta, Finland (e-mail: nikita.uzhegov@spindrive.fi).

A. Smirnov was with the Department of Electrical Engineering, School of Energy Systems, Lappeenranta University of Technology 53850, Lappeenranta, Finland. He is now with the Department of Chemical and Metallurgical Engineering, Aalto University 13000, Espoo, Finland (e-mail: alexander.smirnov@aalto.fi).

C. H. Park is with the Korea Institute of Machinery and Materials, Daejeon 305-343, South Korea (e-mail: parkch@kimm.re.kr).

J. H. Ahn is with MAGNETAR Inc., Daejeon 305-343, South Korea (e-mail: mag@magnetar.co.kr).

J. Heikkinen is with the Department of Mechanical Engineering, School of Energy Systems, Lappeenranta University of Technology 53850, Lappeenranta, Finland (e-mail: janne.e.heikkinen@lut.fi).

J. Pyrhönen is with the Department of Electrical Engineering, School of Energy Systems, Lappeenranta University of Technology 53850, Lappeenranta, Finland (e-mail: juha.pyrhonen@lut.fi).

Color versions of one or more of the figures in this paper are available online at http://ieeexplore.ieee.org.

Digital Object Identifier 10.1109/TIE.2017.2698408

I. Introduction

COMPRESSED air is used in many industrial applications, such as pneumatic actuators, sandblasting, machining, fermentation, instrumentation, air polishing, and many others. Rotary screw compressors have typically been used as the main source of compressed air. However, the recent trend toward oil-free air is limiting their application, and centrifugal compressors are used as a substitute [1]. With centrifugal compressors, the required pressure ratio can be achieved by using several compressor stages. To minimize piping and the number of components, it is favorable to reduce the number of stages. The most compact solution is achieved through two stages on the same shaft. This approach, however, requires a significant power density and high speed (HS), which poses challenges to the design of an electrical machine for such an application.

The power density of an electrical machine increases with the speed [2], [3]. HS machines provide a small footprint and are characterized by high efficiency [4]. With variable frequency drives, it is possible to operate at the desired operating point without a gearbox [5].

In many HS machines, ordinary ball bearings or high-precision ceramic ball bearings are replaced with active magnetic bearings (AMBs) [6], [7]. The AMBs keep the rotor in the air with magnetic forces and without any contact. Furthermore, the friction of these bearings is low. Thus, no lubricant is required, and requirements on cleanliness can be met. Therefore, with this technology, the Class 0 oil-free compressor certification can be achieved according to ISO 8573-1 [8]. The other important advantage is the ability to obtain programmable stiffness and rotor dynamics monitoring [9], [10]. The above-mentioned benefits of an HS machine with magnetic bearings make it an ideal candidate for a two-stage turbocompressor [11].

The benefits come with the cost of a significant effort required for the system development. The design of an HS electrical machine is a complex and multidisciplinary task [12], [13]. In general, one machine cannot be designed universally suitable as each application imposes limitations of its own [14].

The induction machine (IM) and the permanent magnet synchronous machine (PMSM) are two HS machine topologies that are usually selected for a compressor application. The HS PMSM provides a higher efficiency, power factor, and power density than the HS IM [15], [16]. However, the HS IM does

not have permanent magnets (PM), which allows it to operate at higher temperatures and higher rotational speeds thereby extending the power and speed boundaries [17]. The selection of the machine topology is case specific for the air compressor application. A preliminary feasibility study must be conducted to select between the IM and the PMSM based on the requirements, limitations, and preferences.

This paper considers common limitations and requirements of the two-stage compressor set on the electrical machine with AMBs. The study covers examples of a 120-kW, 60 000-r/min IM with a solid rotor and a 225-kW, 50 000-r/min PMSM with a full cylindrical magnet. The main contribution of this paper is the study of the HS IM and HS PMSM drivetrain design aspects, in order to address the limitations imposed by the Class 0 oil-free two-stage air compressor. The design decisions are confirmed by HS PMSM prototype measurements.

II. Design Process

The design process of an HS machine consists of several iterative steps [18]. The design process is based on a list of requirements, and in the case of a two-stage compressor application, it has a number of additional boundary conditions, which are discussed further in this paper. First, a feasibility study is made to verify the concept. The main requirements are specified in terms of power, speed, and minimum motor efficiency required in the operating range to achieve the optimum compression ratio and air volume flow. This provides the initial point for the electrical machine design. Next, based on the rotor weight and rotational speed, the bearing type is selected. At this stage, the machine topology and the location of the impellers are defined. Then, a detailed and iterative analysis of the electrical machine, the AMB design, and the rotordynamics is performed. The main aspects that link all the design steps together are the thermal stability of the system and the dynamics of the rotor. These two characteristics are tightly related to all geometrical dimensions. Finally, the calculation results are compared with the requirements.

A. Limitations and Requirements

Fig. 1 shows two alternatives to place the impellers on the shaft. The first option is to mount both impellers at one end of the electrical machine. This configuration is implemented, for example, in the 500 000 r/min two-stage compressor for the Solar Impulse airplane [19]. In the second option, the impellers are placed at both ends of the electrical machine. In [20], this construction type is implemented for a 300-kW, 60 000-r/min compressor.

The first option is optimal from the cooling point of view. In the compression process, the impellers generate a significant amount of heat, and the rest of the system should be shielded from it. The heat protection is easier to implement when both impellers are attached on one side. The other benefit is that the rotor suffers less from uneven thermal expansion as one end is free to move as a result of thermal expansion. The drawback comes from the unsymmetrical rotor structure, which results in inhomogeneous loads on the bearings. This also further

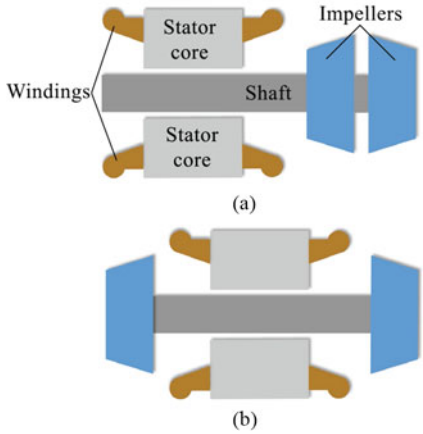

Fig. 1. Impeller arrangement of a two-stage compressor: (a) two impellers are mounted at one end of the machine and (b) impellers are mounted at both ends of the machine.

complicates the rotordynamics and thereby the control of such a rotor-bearing system. Other difficulties arise from the assembly and piping arrangement as part of the piping should provide air inlet along the shaft. This usually leads to an extension of the shaft length.

The second impeller arrangement has a symmetric structure with symmetric load distribution. This provides advantages with respect to the rotordynamics and control. The costs are complications in cooling and problems with thermal expansion. The rotor movement is limited by the axial gaps between the impellers and their housings. From the viewpoint of the compressor, it is beneficial to minimize these gaps. However, uneven expansion of the stator relative to the rotor calls for larger gaps.

Because of the high temperature of the compressed air during operation, the impellers and the impeller housings become additional heat sources for the system. This must be taken into account in the heat transfer analysis of the system.

The orientation of the impellers enables compensation of axial forces. Another option to compensate for the axial force is a vertical design of the system. In this case, the gravity force can compensate for the axial force during operation. However, the axial force varies at different loads and speeds. Therefore, additional control by using AMBs is required to stabilize the system.

In the design of the two-stage compressor, it is necessary to take account of the surge control problem. Precise control of the axial AMB allows implementation of different surge avoidance techniques. For instance, Yoon *et al.* [21] study surge control strategies that apply AMBs. In their work, the experimental results have shown the ability to extend the stable flow range by 21.3% for an industrial centrifugal compressor.

B. HS Machine Design

When the system configuration has been defined and the machine type chosen, it is possible to initiate the detailed electrical machine design. It starts with the selection of the rotor outer diameter and length. The resulting rotor volume must provide the required torque. In general, a larger rotor diameter increases

the peripheral speed, which leads to two major problems. First, a higher rotor peripheral speed increases the rotor stresses and sets more stringent requirements for the components to maintain the rotor integrity. Second, it increases windage losses, which can be dominant at high rotational speeds.

With a long and thin rotor, there is a risk of an overcritical system. In this case, the nominal working point is above the first critical frequency of the rotor, which causes additional control problems. Therefore, the selection of the length/diameter ratio not only plays a critical role in the machine design but also affects the whole compressor assembly.

The initial length/diameter ratio can be calculated using the equations for the IM, χ_{IM}, and the synchronous machine, χ_{SM}, respectively [22],

$$\chi_{\mathrm{IM}} \approx \frac{\pi}{2p}\sqrt[3]{p} \tag{1}$$

$$\chi_{\mathrm{SM}} \approx \begin{cases} \frac{\pi}{4p}\sqrt{p} - & \text{if } p > 1, \\ 1 - 3 - & \text{if } p = 1 \end{cases} \tag{2}$$

where p is the number of pole pairs. Furthermore, the length/diameter ratio can be modified to address the aforementioned problems.

The electromagnetic design of an HS machine must address several critical issues, including extra copper losses because of the skin effect and circulating currents, high core losses at high frequencies, and rotor eddy-current losses because of the air gap flux density harmonics. For example, to avoid losses caused by the skin effect, each individual conductor diameter must be smaller than the penetration depth. A more detailed analysis of the parasitic effects caused by the circulating currents and the ways to overcome them can be found in [23].

In the case of a PMSM, a risk of PM irreversible demagnetization must be assessed in the nominal and overload operation, and during a short circuit. The converter selection and the total harmonic distortion (THD) of the power supply at the rated operating point, and especially at partial loads, have an effect on the machine performance and losses. When selecting a frequency converter, the following technical details should be considered: the control method, switching frequency, capability to install a choke or a filter between the machine and the converter, and the THD of the power supply with and without a choke or a filter. Using these data, it is possible to calculate the machine losses more accurately.

The next design step after the electromagnetic design has been completed and the machine dimensions have been defined is the preliminary calculation of the rotordynamics. The impeller characteristics and the estimated space required for the AMBs and the backup bearings constitute the input information required for this step. After that, the detailed AMB design can be performed.

The machine cooling can be calculated after the frame has been designed. The most common cooling method for a two-stage air compressor is forced air cooling, sometimes combined with stator water jacket cooling. A two-stage compressor has to have a short axial length to avoid problems associated with rotordynamics. This can be achieved through a high integration level of the system and a high machine power density. However, a high integration level leads to a high loss density and can cause overheating of the critical parts and a machine breakdown. Therefore, the cooling design and machine temperature calculations must take account of the impellers, which act as heat sources, and which are thus extremely important in a compact two-stage compressor with a high power density.

There are several methods to calculate the temperature distribution in a system [24], [25]. The lumped parameter method is fast and can be used in initial iterations. In the system heat transfer analysis, it is important to include the impellers as temperature boundary conditions in the model. The fluid dynamics FEM calculations provide more accurate results but require significant computation resources.

C. AMB Design

The common trend for AMBs is to minimize their dimensions, especially the axial dimension, and to minimize the power losses. The first target is important in order to increase the frequency of the rotor flexible modes to achieve subcritical operation, or at least to reduce the number of modes crossed during a run-up. The second target is to mitigate the cooling problems and increase the overall efficiency of the system.

For machines with high rotational speeds, roughly above 30 000 r/min, the eddy currents in the rotor lamination stack should be considered. The field provided by the bearings is not rotating with the machine, and thus, the rotor faces significant flux changes. In traditional heteropolar magnetic bearings, this might lead to a reduced load capacity above a certain speed level and coupling between the axes [26]. Both of these effects are undesirable. To overcome the issue, a homopolar type of bearing is applied. In that case, the flux travels through the rotor surface only in one direction, thereby reducing the eddy currents and increasing the bandwidth.

A compact homopolar solution is a hybrid bearing with PM biasing. The magnet provides an initial flux density, which is later adjusted in the desired direction with control coils. In that way, both control coils can be made smaller, the total current in the windings is reduced, and thus, resistive losses are minimized [26].

A schematic of heteropolar and homopolar bearings is presented in Fig. 2. The heteropolar bearing has eight poles, and the flux bias is provided by the bias current. In that case, the flux travels from one pole to another through the rotor surface in the radial direction. The homopolar bearing uses the PM to provide the initial bias flux, and the control coils can change the flux balance. The flux passes through the rotor in an axial plane and flows into the poles with the same direction pointing from the inside of the rotor to the outer surface. In Fig. 2, the hybrid structure that combines the axial and radial bearings is demonstrated. In the axial part, the flux is controlled with an axial coil that defines through which leg the flux will flow. Therefore, it determines the direction of the axial force. If an axial bearing is not needed, it is replaced by a solid steel part, which is usually referred to as a "dead leg."

In addition, the hybrid structure provides an opportunity to minimize the required power electronics. Instead of ten

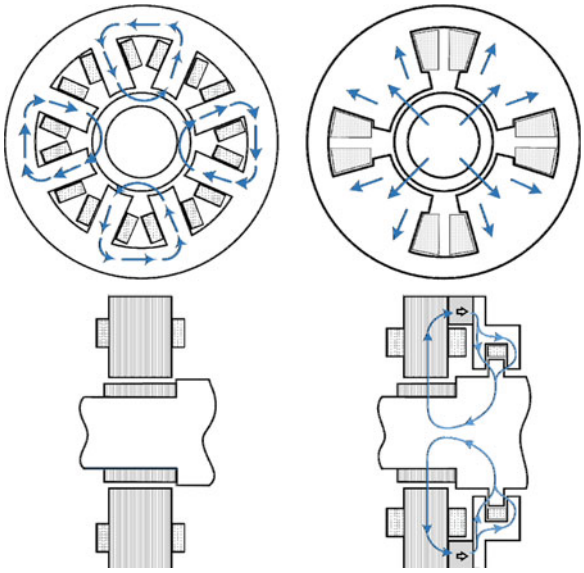

Fig. 2. Radial and axial cross sections of magnetic bearings. On the left, there is a typical heteropolar bearing with current biasing and eight poles. On the right, there is a hybrid combined axial and radial bearing with PM biasing. The blue lines indicate the flux path.

current channels for a typical heteropolar (axial + two radial bearings) arrangement, the number of current sources is reduced to five.

A typical radial heteropolar bearing with bias current to provide force in any direction has two pairs of electromagnets. Each pair is placed along one axis to provide attractive forces in the opposite direction. To ensure linear operation, the magnets are supplied with bias current. Thus, to produce force, the current in one electromagnet is reduced by some proportion while the current is increased by the same proportion in the opposite electromagnet. A common way to achieve this behavior is to have a separate current source for each electromagnet. Consequently, there are four sources for one radial bearing. There is an alternative solution where the bias is provided by a separate winding for all electromagnets; thus, for the control of each pair, one power source is used. It changes the force by altering the flux in both electromagnets simultaneously but in a different direction. In that case, for one radial bearing, the total number of amplifiers is reduced to two and an additional one for the bias current. A similar principle is used for bearings with PM biasing, but the bias amplifier and the bias winding are eliminated as the flux is provided by the magnets. The axial bearing behaves in a similar way, and it can operate with the PM bias flux and only one power amplifier.

III. Case Studies

A. Induction Machine

The first case study is a 120-kW, 60 000-r/min IM with hybrid AMBs. The machine has an axially slitted solid rotor with conducting end rings at both rotor ends. The conducting end rings significantly enhance the efficiency and power factor of the solid rotor IM. The machine is a 2-pole configuration and has 24 stator slots. The key design parameters of this machine are illustrated in Table I. The rotational speed of 60 000 r/min and the rotor outer diameter of 76 mm lead to the rotor peripheral speed of 239 m/s, which sets strict requirements on the mechanical rigidity of the rotor. The rotor structure is shown in Fig. 3.

TABLE I
Key IM Parameters

Parameter	Value
Rated speed, r/min	60 000
Rated power, kW	120
Pole pairs	1
Rated voltage, V	400 (Star)
Rated current, A	267
Number of stator slots	24
Stack length, mm	120
Rotor outer diameter, mm	76
Stator outer diameter, mm	184
Stator core material	M250-35A
Rotor core material	Imacro M
End ring material	Glidcop 15

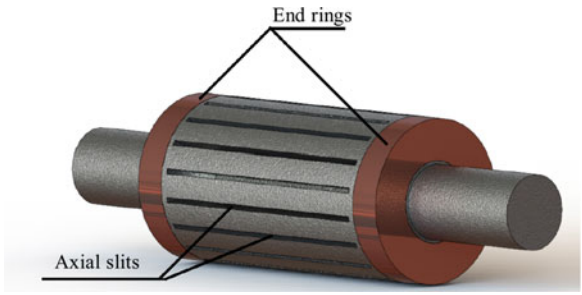

Fig. 3. 3-D model of the solid rotor with axial slits and conducting end rings.

There are two major structural mechanical limitations in this machine topology. The first one is related to the axial slits. The purpose of these slits is to reduce the surface resistance and intensify flux penetration into the rotor. This leads to lower electromagnetic losses and a higher machine power factor. The electromagnetic performance is enhanced as the slit depth increases. However, the mechanical rigidity decreases with deeper slits. Therefore, it is important to find a balance between the mechanical and electromagnetic boundaries. A study to find the electromagnetically optimal slit dimensions for a solid rotor IM has been conducted for instance by Huppunen in [27].

Fig. 4 shows the stress distribution in one of the rotor slits of the IM under study. According to a three-dimensional finite element method (FEM) analysis, the slit bottom radius significantly affects the maximum stresses. In the FEM analysis, special attention is paid to meshing, which has to be fine enough to provide convergent results from such local stress distribution. In the design under consideration, the slit bottom fillet radius of 1 mm provides a stress level below 400 MPa at the rated operating point with the material yield strength of 700 MPa providing a safety margin of 1.75 to ensure durability against unexpected additional forces and a sufficient lifetime expectancy. Because

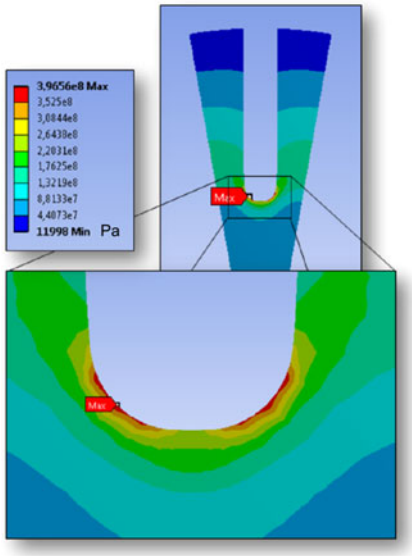

Fig. 4. Stress distribution in the slits of the IM in the rated operating conditions and 5% overspeed.

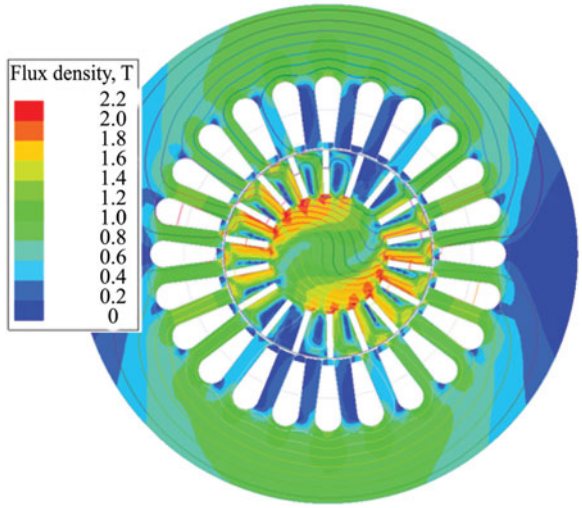

Fig. 5. Flux density distribution and the flux lines at the rated operating point in the 120-kW IM.

TABLE II
LOSS DISTRIBUTION IN THE IM

Loss Location	Losses, W	Loss Share, %
Copper	1192	17
Rotor	1665	24
Rotor outer surface	1616	24
Core	1746	26
Additional	600	9
Total	6819	100

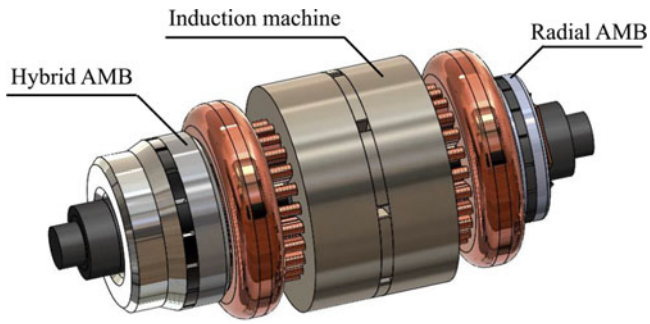

Fig. 6. Models of the IM and the AMBs.

of the importance of the slit bottom fillet radius, at the manufacturing stage, special attention has to be paid to the selection of the work tool as it strongly affects the maximum stresses of the structure.

The second structural limitation is related to the end rings. The maximum stresses occur on the border of the solid rotor and the inner surface of the conducting end ring. In the machine under study, the material Glidcop 15 was selected for the conducting end rings because it has a high conductivity and a suitable yield strength, which is also maintained at high temperatures. Precise assembly of the end rings is one of the key factors affecting the rotor rigidity at high peripheral speeds.

The electromagnetic design of the 120-kW IM was performed by applying 2-D FEM software taking into account the 3-D phenomena by the methodology presented in [28]. A comparison of the 3-D and 2-D FEM analyses for an HS IM can be found in [29]. Fig. 5 shows the machine cross section, flux lines, and flux density distribution in the IM at the rated operating point. The rotor is saturated under the slits, which is a typical situation for an axially slitted rotor. The calculated power factor at the nominal operating point is 0.71.

Table II illustrates the electromagnetic loss distribution in the IM at the rated point. The copper losses are calculated with a temperature rise of 120 °C. Extra copper losses can be taken into account by the method presented in [30]. For the core losses, the Steinmetz equation was used. Because of the solid rotor structure, the rotor losses constitute about half of the total electromagnetic losses. In Table II, the rotor outer surface refers to the layer having a thickness equal to the penetration depth. The losses on the rotor outer surface account for about 24% of the total machine losses. This is due to the high harmonic content of the air gap flux density. The additional losses are calculated as 0.5% of the output power. The losses from the magnetic bearings are estimated to be around 82 W. The electromagnetic efficiency of the proposed machine is about 94%.

Fig. 6 shows the model of the IM with AMBs. The bearings are represented by two parts. The first one is a hybrid bearing that combines the axial and radial bearings into a single unit, and the second is a radial homopolar bearing with a dead leg. Both bearings provide a bias flux with a PM ring in the stator part. The ring is segmented into separate elements to simplify the manufacturing process. The geometry selection for such bearings is discussed in detail in [31].

The bending modes of the free–free rotor with impellers were estimated by the FEM. For rotor modeling, Timoshenko beam elements were applied. At standstill, the first two bending mode pairs have frequencies of 574 Hz and 954 Hz. At the nominal

point, the machine operates in the supercritical region between the second backward mode and the second forward mode. The separation from the modes is around 150 Hz (15%), which provides both enough safety margin and a reasonable operating range, as the operating range for the compressor application has quite small variations from the nominal speed.

One of the requirements for the bearings in compressor applications is to provide a high enough axial force in all operating conditions. Although this force is balanced by the impeller design, in most cases, the balancing is done for the nominal point. For partial load operation, the axial force difference can reach a significant absolute value.

The traditional axial C-shape bearing leads to a large diameter of the axial disc. This diameter is limited by the material strength, which is low for magnetic materials in most cases. For the homopolar hybrid bearings, the disc diameter is significantly smaller; however, there is a limitation on the minimum possible rotor diameter. The flux from the axial to the radial bearing travels through the rotor core. Therefore, the rotor surface cross section should provide a path for the magnetic flux without saturation to produce the required force. In general, the axial force in a compressor application is greater than the radial one, as there are no major external disturbances in the radial direction. The flux that produces the axial force is then divided between two radial directions. Thus, the force capacity in a combined hybrid bearing between the axial and radial bearings is close to 2:1 [31]. It can be concluded that the bearing design is dominated by the axial force requirement.

One limitation of the rotor structure for the IM is imposed by the inner diameter of the end rings. This significantly reduces the possible shaft diameter outside the active part. The first consequence is that the rotor is more flexible. For the system under consideration, this results in a supercritical nominal operation point, which is located between the first and second flexible modes. Supercritical machines are more sensitive to the rotor balancing and manufacturing accuracy, and require a more advanced control for magnetic bearings [9]. In general, all these effects are undesirable. The second effect of the limitation on the maximum shaft diameter is that it conflicts with the above-mentioned requirement for the minimum rotor surface area. If a reasonable tradeoff is not possible, another type of axial bearing should be applied. As a classical C-shape axial bearing results in a significant disc diameter, there is an option to use a PM biased axial bearing not combining it with the radial bearing [32]. Therefore, the requirement of the inner surface area of the rotor is relaxed.

B. Permanent-Magnet Synchronous Machine

The second case study is a 225-kW, 50 000-r/min PMSM. This machine is designed for a two-stage turbo compressor shown in Fig. 7 [33]. It consists of upper and lower impellers, a rotor shaft, magnetic bearings, and an electrical machine. A detailed analysis of the designed AMBs is presented in [32] and [34]. The rotor shaft is a shrink-fitted assembly of a full cylindrical magnet, SUS 304 shaft studs, and an Inconel 718 sleeve. Because of the high thermal resistance of the carbon

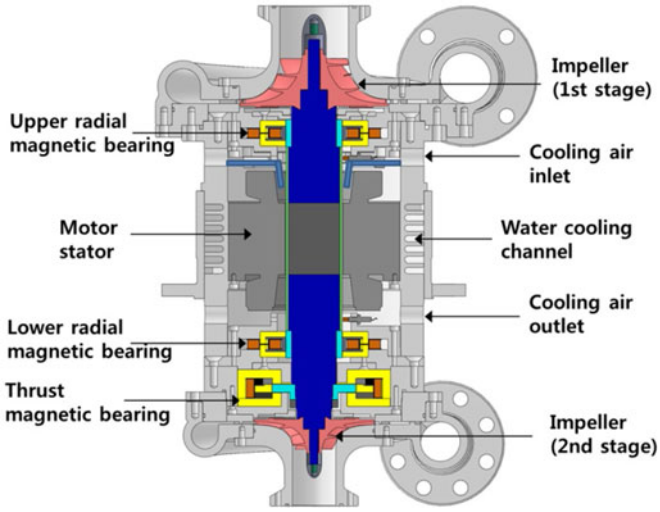

Fig. 7. Configuration of the 225-kW, 50 000-r/min turbo compressor.

TABLE III
KEY PMSM PARAMETERS

Parameter	Value
Rated speed, r/min	50 000
Rated power, kW	225
Pole pairs	1
Rated voltage, V	380 (Star)
Maximum current, A	570
Number of stator slots	36
Stack length, mm	88.5
Rotor outer diameter, mm	70.2
Physical air gap length, mm	1.2
Stator outer diameter, mm	192
Stator core material	25PN1500
Magnet material	NdFeB
Rotor sleeve material	Inconel 718

fiber sleeve, it could not be applied in the machine under study. The compressor housing has a water cooling channel to cool the motor stator, and the inlet and the outlet are designed to supply cooling air both to the rotor and motor stator. The machine has a two-pole design and 36 stator slots. The key design parameters of this machine are illustrated in Table III.

The PM material selected for the machine is NdFeB, the tensile strength of which is only 80 MPa, making it the weakest part of the rotor. Therefore, an appropriate sleeve thickness and a suitable shrink fit of the sleeve around the magnet should be found to protect the magnet against centrifugal forces at 50 000 r/min. Fig. 8 shows the stress analysis results over the magnet and the sleeve for the sleeve thickness of 3.1 mm and the diametral interference of 200 μm at the rotational speed of 52 000 r/min. The maximum stress is around 58 MPa at the center of the magnet, which leads to a safety factor of 1.38. The thickness of the sleeve is selected conservatively to reach the safety margin of 2.0 in order to ensure a mechanical design that withstands operational loads in the prototype testing process.

The frequency of the free–free first bending mode for the rotor including impellers is predicted to be at 1269 Hz. A rotor

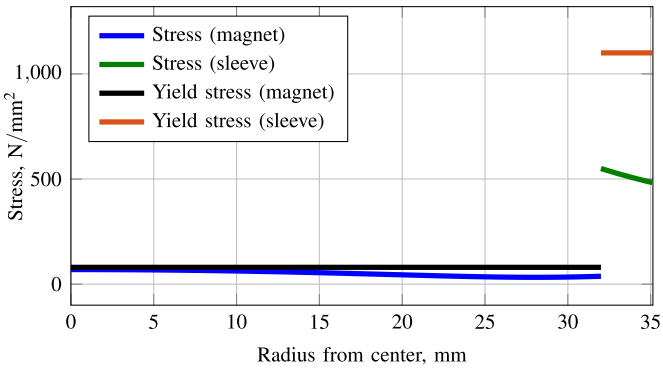

Fig. 8. Von Mises stress over the magnet and the sleeve at 52 000 r/min (4% overspeed).

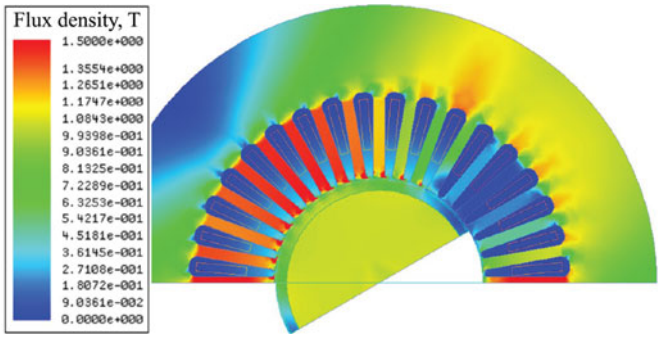

Fig. 9. Flux density distribution at the rated operating point in the 225-kW PMSM.

TABLE IV
ELECTROMAGNETIC LOSS DISTRIBUTION IN THE PMSM

Loss Location	Losses, W	Loss Share, %
Copper	958	37
Rotor	827	31
Core	834	32
Total	2619	100

dynamic analysis was performed using a commercial program XLRotor. It is predicted that the critical speed in the rigid body modes will be less than 5000 r/min, and that the first backward bending will take place at 70 000 r/min, which has a sufficient margin to the rated speed of 50 000 r/min.

The electromagnetic design of the 225-kW PM machine was performed using the 2-D FEM software. Fig. 9 shows the cross section and flux density distribution in the PMSM at the rated operating point. To limit the iron losses, the maximum value of the flux density in the teeth does not exceed 1.5 T. In addition, the stator yoke is made thick to enable a low yoke flux density. The back electromotive force (EMF) constant and torque constant of the designed PMSM are expected to be $0.0509\ \mathrm{V/(reds)}$ and $0.0763\ \mathrm{N{\cdot}m/A}$, respectively. The peak and rms currents are expected to be 570 A and 400 A, respectively. The power factor at the nominal operating point is 0.90.

Table IV presents the electromagnetic losses in the 225-kW PMSM at the rated operating point. The rotor losses constitute

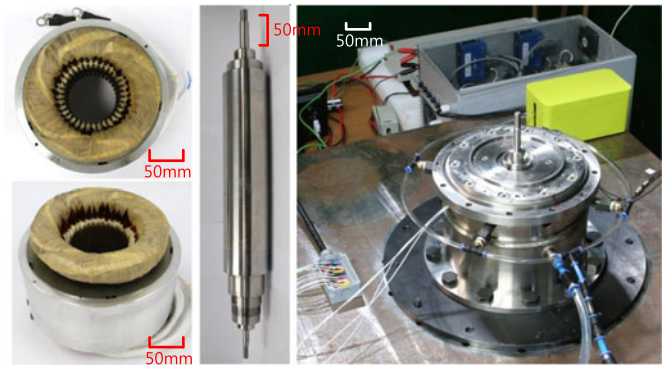

Fig. 10. Constructed stator and assembled compressor housing for the no-load PMSM test.

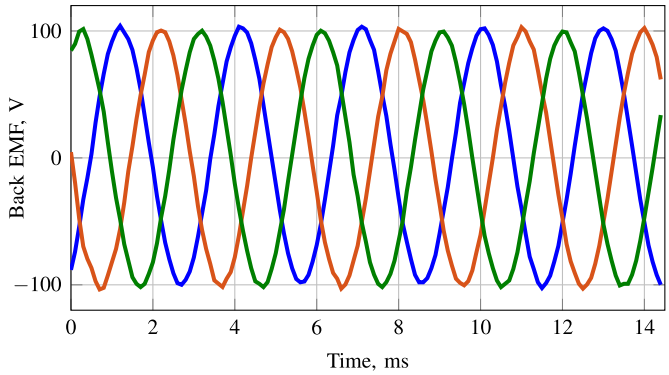

Fig. 11. Measured back EMF of the three phases at 20 000 r/min for the PMSM prototype.

a significant proportion of the total losses. To avoid the risk of irreversible PM demagnetization, the air cooling is guided directly to the air gap to keep the rotor temperature low. Because of the low flux density levels in the stator, the iron losses are kept below 1000 W even at the 833 Hz nominal supply frequency. The calculated windage losses for the shaft without impellers are about 1.8 kW according to the procedure presented in [9].

IV. PROTOTYPE TEST RESULTS

Fig. 10 shows the constructed stator and the assembled compressor, which does not have impellers for a no-load test. First, the motoring test was performed in the no-load condition to evaluate the structural strength of the shaft. The rotational speed of the shaft can be stably increased up to 51 000 r/min, which verifies that the shaft has a sufficient structural strength. Fig. 11 shows the back EMFs of the three phases, which were measured at 20 000 r/min during spin-down. The peak value of the measured back EMF is 102 V, and the error is 2.5% compared with the predicted value based on the results calculated using the back EMF constant. The calculated and measured phase resistances at the rated temperature are 2 mΩ and 2.1 mΩ, respectively.

Next, the motoring test was performed in the load condition for the rotor with impellers. The rotor with impellers and the experimental setup are shown in Fig. 12. In the load condition with

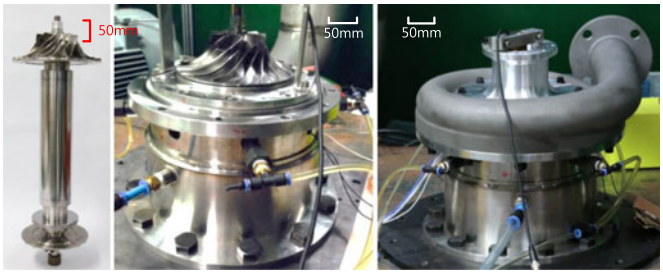

Fig. 12. Rotor and compressor without and with a volute for the 225-kW PMSM prototype load test.

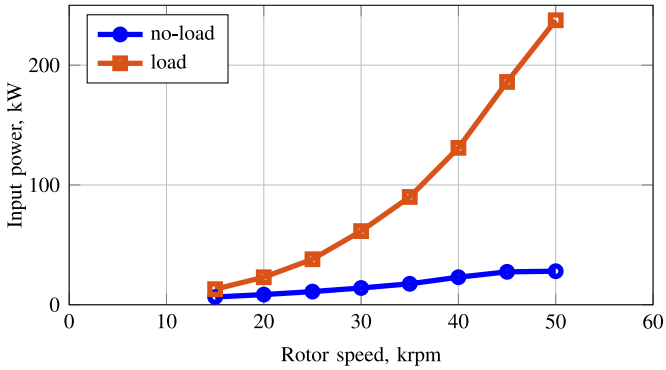

Fig. 13. Measured motor input power with a varying rotor speed for the 225-kW PMSM no-load and load tests.

an elevated rotational speed (see Fig. 13), both the motor input power and the temperatures of the stator and the rotor increased rapidly. Therefore, it is necessary to provide a sufficient amount of cooling air and liquid coolant to keep the PMSM temperatures below the critical level. The flow rate of the cooling air was controlled to maintain the temperature of the motor stator below 100 °C. Several thermocouples were installed inside the compressor to measure the temperature around the motor and the magnetic bearings, and the inlet and outlet temperatures of the compressor. Sufficient cooling is important to avoid winding overheating, irreversible PM demagnetization, and a reduction in the back EMF. In addition, the rotor and stator temperature rises must be commensurate to avoid unequal thermal expansion of the rotating and stationary parts. In the full-load condition, the rotor speed is increased to 50 000 r/min. The measured motor input power with respect to the rotor speed in the no-load and load conditions are shown in Fig. 13. At 50 000 r/min, the PMSM input power is 28 kW in the no-load test and 237.5 kW at the nominal load. The measured power factor at the nominal load is 0.88, which is in a good agreement with the simulated value.

Because the electromagnetic losses in the rated operation in Table IV are significantly lower compared with the input power for the no-load test, we may conclude that there are high mechanical losses, such as windage losses. Another reason for the high measured losses is related to the converter supply and the absence of filters between the converter and the machine. The measured THD value for the phase current in the prototype was 34% at 30 000 r/min. In addition, extra copper and core losses compared with the simulated values are possible in the prototype because of the high supply frequency. Therefore, about 30 kW of electromagnetic and mechanical losses should be considered when determining the output power of the compressor.

The bearing losses were estimated by measuring the input current and voltage of the dc power supply with a power meter. This method gives the full power consumption of the magnetic bearings and the power electronics. The voltage is 150 V, and the current is 1.5 A, resulting in 225 W losses.

V. Conclusion

In this paper, the main design aspects of an HS electrical machine supported by AMBs for an air compressor were demonstrated. The key limitations of the selected application were described. This paper showed how the system configuration including the impeller location, the horizontal or vertical shaft positioning, and the electrical machine type affects the limitations. The main design challenges for electrical machine and AMB designers from electromagnetic, mechanical, thermal, and control viewpoints were listed. The advantages of the hybrid AMBs for the two-stage compressor were described.

The two case studies illustrated how the design challenges are addressed in the case of an IM and a PMSM supported by AMBs. The key mechanical limitations of both topologies are related to the specific rotor construction and must be assessed considering an overspeed operation and a temperature rise. A PMSM can provide a significantly more compact solution compared with the IM if a proper cooling of the system can be arranged. In the machines under study, it leads to overcritical IM and undercritical PMSM operation. Mechanical losses and extra electromagnetic losses caused by the high frequency in the windings and in the stator must be accurately calculated to define the output compressor power and ensure sufficient cooling.

Because of the high integration level, a feasible HS drivetrain design for a two-stage oil-free air compressor is possible only with a systematic approach when the mutual influence of the components is taken into account.

References

[1] S.-M. Jang, H.-W. Cho, and S.-K. Choi, "Design and analysis of a high-speed brushless DC motor for centrifugal compressor," *IEEE Trans. Magn.*, vol. 43, no. 6, pp. 2573–2575, Jun. 2007.

[2] S. Singhal, "Electric drive compressor systems: High-speed turbo compressors used in the oil and gas industry," *IEEE Ind. Appl. Mag.*, vol. 20, no. 6, pp. 52–63, Nov./Dec. 2014.

[3] Z. Huang and J. Fang, "Multiphysics design and optimization of high-speed permanent-magnet electrical machines for air blower applications," *IEEE Trans. Ind. Electron.*, vol. 63, no. 5, pp. 2766–2774, May 2016.

[4] A. Tenconi, S. Vaschetto, and A. Vigliani, "Electrical machines for high-speed applications: Design considerations and tradeoffs," *IEEE Trans. Ind. Electron.*, vol. 61, no. 6, pp. 3022–3029, Jun. 2014.

[5] S. Silber, J. Sloupensky, P. Dirnberger, M. Moravec, W. Amrhein, and M. Reisinger, "High-speed drive for textile rotor spinning applications," *IEEE Trans. Ind. Electron.*, vol. 61, no. 6, pp. 2990–2997, Jun. 2014.

[6] P. Cui, S. Li, Q. Wang, Q. Gao, J. Cui, and H. Zhang, "Harmonic current suppression of an AMB rotor system at variable rotation speed based on multiple phase-shift notch filters," *IEEE Trans. Ind. Electron.*, vol. 63, no. 11, pp. 6962–6969, Nov. 2016.

[7] S. Zheng, Q. Chen, and H. Ren, "Active balancing control of AMB-rotor systems using a phase-shift notch filter connected in parallel mode," *IEEE Trans. Ind. Electron.*, vol. 63, no. 6, pp. 3777–3785, Jun. 2016.
[8] *Compressed Air—Part 1: Contaminants and Purity Classes*, ISO 8573–1:2010, 2010.
[9] G. Schweitzer and E. H. Maslen, *Magnetic Bearings*. Heidelberg, Germany: Springer, 2009.
[10] R. J. Madden, J. T. Sawicki, and A. H. Pesch, "Model validation for identification of damage dynamics," *J. Eng. Gas Turbines Power*, vol. 137, no. 6, Jun. 2015, Art. no. 062506.
[11] B. Han, Q. Xu, and Q. Yuan, "Multi-objective optimization of a combined radial-axial magnetic bearing for magnetically suspended compressor," *IEEE Trans. Ind. Electron.*, vol. 63, no. 4, pp. 2284–2293, Apr. 2016.
[12] Z. Huang, J. Fang, X. Liu, and B. Han, "Loss calculation and thermal analysis of rotors supported by active magnetic bearings for high-speed permanent-magnet electrical machines," *IEEE Trans. Ind. Electron.*, vol. 63, no. 4, pp. 2027–2035, Apr. 2016.
[13] D. Gerada, A. Mebarki, N. L. Brown, C. Gerada, A. Cavagnino, and A. Boglietti, "High-speed electrical machines: Technologies, trends, and developments," *IEEE Trans. Ind. Electron.*, vol. 61, no. 6, pp. 2946–2959, Jun. 2014.
[14] F. Zhang, G. Du, T. Wang, F. Wang, W. Cao, and J. L. Kirtley, "Electromagnetic design and loss calculations of a 1.12-MW high-speed permanent-magnet motor for compressor applications," *IEEE Trans. Energy Convers.*, vol. 31, no. 1, pp. 132–140, Mar. 2016.
[15] Z. Kolondzovski, A. Arkkio, J. Larjola, and P. Sallinen, "Power limits of high-speed permanent-magnet electrical machines for compressor applications," *IEEE Trans. Energy Convers.*, vol. 26, no. 1, pp. 73–82, Mar. 2011.
[16] A. J. Grobler, S. R. Holm, and G. van Schoor, "A two-dimensional analytic thermal model for a high-speed PMSM magnet," *IEEE Trans. Ind. Electron.*, vol. 62, no. 11, pp. 6756–6764, Nov. 2015.
[17] M. Dems and K. Komeza, "Performance characteristics of a high-speed energy-saving induction motor with an amorphous stator core," *IEEE Trans. Ind. Electron.*, vol. 61, no. 6, pp. 3046–3055, Jun. 2014.
[18] N. Uzhegov, E. Kurvinen, J. Nerg, J. Pyrhönen, J. T. Sopanen, and S. Shirinskii, "Multidisciplinary design process of a 6-slot 2-pole high-speed permanent-magnet synchronous machine," *IEEE Trans. Ind. Electron.*, vol. 63, no. 2, pp. 784–795, Feb. 2016.
[19] D. Krahenbuhl, C. Zwyssig, H. Weser, and J. W. Kolar, "A miniature 500000-r/min electrically driven turbocompressor," *IEEE Trans. Ind. Appl.*, vol. 46, no. 6, pp. 2459–2466, Nov./Dec. 2010.
[20] J. F. Gieras and J. Saari, "Performance calculation for a high-speed solid-rotor induction motor," *IEEE Trans. Ind. Electron.*, vol. 59, no. 6, pp. 2689–2700, Jun. 2012.
[21] S. Y. Yoon, Z. Lin, and P. E. Allaire, "Experimental evaluation of a surge controller for an AMB supported compressor in the presence of piping acoustics," *IEEE Trans. Control Syst. Technol.*, vol. 22, no. 3, pp. 1215–1223, May 2014.
[22] J. Pyrhönen, T. Jokinen, and V. Hrabovcova, *Design of Rotating Electrical Machines*. Chichester, UK: Wiley, 2008.
[23] M. van der Geest, H. Polinder, J. Ferreira, and D. Zeilstra, "Current sharing analysis of parallel strands in low-voltage high-speed machines," *IEEE Trans. Ind. Electron.*, vol. 61, no. 6, pp. 3064–3070, Jun. 2014.
[24] J. Nerg, M. Rilla, and J. Pyrhonen, "Thermal analysis of radial-flux electrical machines with a high power density," *IEEE Trans. Ind. Electron.*, vol. 55, no. 10, pp. 3543–3554, Oct. 2008.
[25] A. Boglietti, A. Cavagnino, and D. Staton, "Determination of critical parameters in electrical machine thermal models," *IEEE Trans. Ind. Appl.*, vol. 44, no. 4, pp. 1150–1159, Jul./Aug. 2008.
[26] A. Filatov and L. Hawkins, "Comparative study of axial/radial magnetic bearing arrangements for turbocompressor applications," *Proc. Inst. Mech. Eng., J. Syst. Control Eng.*, vol. 230, no. 4, pp. 300–310, Apr. 2016.
[27] J. Huppunen, "High-speed solid-rotor induction machine–electromagnetic calculation and design," Ph.D. dissertation, Dept. Elect. Eng., Lappeenranta Univ. Technol., Lappeenranta, Finland, 2004.
[28] J. Pyrhönen, J. Nerg, P. Kurronen, and U. Lauber, "High-speed high-output solid-rotor induction-motor technology for gas compression," *IEEE Trans. Ind. Electron.*, vol. 57, no. 1, pp. 272–280, Jan. 2010.
[29] M. V. Terzic, D. S. Mihic, and S. N. Vukosavic, "Impact of rotor material on the optimal geometry of high-speed drag-cup induction motor," *IEEE Trans. Energy Convers.*, vol. 31, no. 2, pp. 455–465, Jun. 2016.
[30] J. A. Ferreira, "Improved analytical modeling of conductive losses in magnetic components," *IEEE Trans. Power Electron.*, vol. 9, no. 1, pp. 127–131, Jan. 1994.
[31] Y. Le and K. Wang, "Design and optimization method of magnetic bearing for high-speed motor considering eddy current effects," *IEEE/ASME Trans. Mechatronics*, vol. 21, no. 4, pp. 2061–2072, Aug. 2016.
[32] C. H. Park, S. K. Choi, and S. Y. Ham, "Design of magnetic bearing for turbo refrigerant compressors," *Mech. Ind.*, vol. 15, no. 4, pp. 245–252, Jun. 2014.
[33] C. H. Park and J. Y. Park, "Design and experiment of 300-HP-class turbo compressor with hybrid magnetic bearings," in *Proc. 15th Int. Symp. Mag. Bearings*, Aug. 2016, pp. 1–6.
[34] C. H. Park, S. H. Kim, and K. S. Kim, "Vacuum chamber-free centrifuge with magnetic bearings," *Rev. Sci. Instrum.*, vol. 84, no. 9, Sep. 2013, Art. no. 095106.

Nikita Uzhegov (M'14) received the M.Sc. and D.Sc. degrees in electrical engineering from Lappeenranta University of Technology (LUT), Lappeenranta, Finland, in 2012 and in 2016, respectively.

He was a Researcher with the School of Energy Systems, LUT, from 2012 to 2016. He is the cofounder of SpinDrive, Lappeenranta, Finland, where he is currently a High-Speed Electrical Machine Designer. His current research focuses on high-speed electrical machines and materials used in electrical machines.

Alexander Smirnov (M'05) received the M.Sc. and D.Sc. degrees in electrical engineering from Lappeenranta University of Technology (LUT), Lappeenranta, Finland, in 2008 and in 2012, respectively.

He was a Postdoctoral Researcher with LUT from 2012 to 2016. He is currently a Postdoctoral Researcher at Aalto University, Espoo, Finland. His main research interests include high-speed electrical machines and drives, active magnetic bearings, and process control and optimization.

Cheol Hoon Park was born in South Korea in 1973. He received the B.S. and M.S. degrees in mechanical engineering from Yonsei University, Seoul, South Korea, and the Ph.D. degree in mechanical engineering from the Korea Advanced Institute of Science and Technology, Daejeon, South Korea.

He was with the Hard Disk Drive (HDD) Division, Samsung Electronics, in 2000. In 2007, he joined the Korea Institute of Machinery and Materials (KIMM), Daejeon, South Korea, where he is currently a Principal Researcher in the Department of Robotics and Mechatronics. His research interests include magnetic bearings, high-speed rotating machines, precision control, and artificial muscles.

Ji Hun Ahn was born in Pohang, South Korea, in 1984. He received the M.S. degree in electrical engineering in 2012 from Chungnam National University, Daejeon, South Korea, where he is currently working toward the Ph.D. degree in the Department of Electrical Engineering.

He is currently a Principal Researcher at MAGNETAR Inc., Daejeon, South Korea, investigating high-speed permanent-magnet motors. His research focuses on high-speed permanent-magnet synchronous motors with hybrid magnetic bearings.

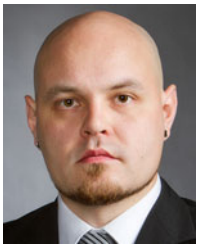

Janne Heikkinen received the M.Sc. degree in mechanical engineering and the D.Sc. degree from Lappeenranta University of Technology (LUT), Lappeenranta, Finland, in 2010 and 2014, respectively.

He is currently a Postdoctoral Researcher in the Laboratory of Machine Dynamics, LUT. His research interests include the field of rotating electric machines, in particular, high-speed machinery. His main expertise is on rotordynamics, structural vibrations, and vibration measurements.

Juha Pyrhönen (M'06) was born in Kuusankoski, Finland, in 1957. He received the D.Sc. degree from Lappeenranta University of Technology (LUT), Lappeenranta, Finland, in 1991.

He became a Professor of electrical machines and drives at LUT in 1997. He is engaged in research and development of electric motors and power-electronic-controlled drives. He has wide experience in the research and development of special electric drives for distributed power production, traction drives, and high-speed applications. Permanent-magnet materials and their application in machines play an important role in his research. His current research focuses on new carbon-based materials for electrical machines.